Asian Journal of Chemistry; Vol. 35, No. 3 (2023), 712-716

ASIAN JOURNAL OF CHEMISTRY

https://doi.org/10.14233/ajchem.2023.27566

Microwave-Assisted Synthesis of Ceria-Zirconia Nanoparticles: Characterization and their Antimicrobial Studies

TAMILSELVI RAMASAMY[1] and THIRUMOORTHI ARUNACHALAM[2,*]

[1]Research and Development Centre, Bharathiar University, Coimbatore-641046, India
[2]Department of Chemistry, Government Arts College, Udumalpet-642126, India

*Corresponding author: E-mail: dramoorthiudt@gmail.com

Received: 11 January 2023; *Accepted*: 7 February 2023; *Published online*: 27 February 2023; AJC-21165

Ceria-zirconia (CZAA) nanoparticles with varied molar ratio of 1:1, 0.8:0.2, 0.6:0.4, 0.4:0.6 and 0.2:0.8 labelled as CZAA-0, CZAA-1, CZAA-2, CZAA-3 and CZAA-4 were prepared using cerium nitrate, zirconium nitrate and ascorbic acid as promoter. The X-ray diffraction, scanning electron microscopy, ultraviolet-visible, Raman and Fourier transform infrared spectra were used to characterize the prepared nanoparticles. The prepared CZAA nanoparticles were tested for antibacterial activity against *Escherichia coli*, *Klebsiella pneumonia*, *Staphylococcus aureus* and *Enterococcus faecalis* bacterial strains as well as *Aspergillus niger*, *Penicillium* and *Candida albicans* fungal strains using the well diffusion method. They were shown to be highly antimicrobial agents to all pathogenic strains tested.

Keywords: Ceria-Zirconia nanoparticles, Microwave synthesis, Ascorbic acid, Antibacterial activity, Antifungal activity.

INTRODUCTION

Nanomaterials, the word which revolutionized the scientific world since its inception is promising in various applications in the broad area of science and technology. Among them, metal nanoparticles have gathered a special interest with its size-dependent and morphological properties enlarging the potential applications in several fields [1-4]. Various preparatory techniques are used to synthesize the nanoparticles such as chemical [5], photochemical [6], electrochemical [7] and biological methods [8]. But the synthetic techniques have its own concerns with the harmful chemicals and ambience required at times. While steps like limiting the chemical use as capping and/or reducing agent don't improve considerably, they are nonetheless important. Thus, the preparation of such materials with minimal environmental damage, economic viability and energy efficiency is a demand in the growing industrial society. In such circumstances, the synthesis *via* microwave assisted techniques are looked over for its simplicity, efficiency and cost-effectiveness. As mentioned earlier, the rapid, simple and cost-effectiveness of microwave heating techniques are often considered for high-yield and purity products [9]. Such characteristics made microwave based synthesis common in recent times for synthetic organic and solution phase chemistry [10-13]. The instantaneous growth in this field of research over the years has evolved into novel material synthesis and has the potential to feature as a standardized technique in solid-state synthesis.

In recent time, CO oxidation at lower temperatures is often looked over for its extensive applications in automobile industries and proton exchange membrane fuel cells [9]. Precious metal-based catalysts are well-known for their high activity and stability in oxidation processes and are commonly employed for CO oxidation [14]. Due to the expense of precious metals and their susceptibility to sulphur poisoning, efforts have been focused on enhancing the catalytic performance of metal oxide-based catalysts [15].

Cerium oxide is known for its numerous applications that include heterogeneous catalysis in automobile exhaust gas conversion [16], solid-oxide fuel cells [17], gas sensors [18], semiconductor fabrications [19] and issues related with spinal cord repair and other central nervous system illness [20]. Further, it is a highly refractive ceramic with a high melting point of 2400 ºC. When its size is reduced to nanoscale, it has an improved behaviour in not only the physical, chemical and electrical characteristics, but also a high thermodynamic affinity for oxygen and sulphur. Like any other material, CeO_2 has its own

concerns with degradation at high operating temperatures, which hinders its continuous usage with low oxygen storage capacity. Further, mixed metal oxides such as addition of metallic and non-metallic oxides especially copper [21], zirconium and titanium [22] with ceria is carried out for increased performance. Consequently, the current study is focused on the preparation of ceria-zirconia nanoparticles in different molar ratio *via* microwave assisted synthesis. The prepared samples were characterized by various characterization techniques such as UV-visible, FT-IR, Raman, XRD and SEM analysis. Further, the antimicrobial activities were also evaluated.

EXPERIMENTAL

Nitrates are known to help combustion reactions, hence cerium nitrate and zirconyl nitrate were chosen as source materials. In current work, desired quantities of cerium(III) nitrate [$Ce(NO_3)_3{\cdot}6H_2O$] (Aldrich, 99%) and zirconyl(IV) nitrate [$ZrO(NO_3)_2{\cdot}2H_2O$] (Aldrich, 99%) were dissolved in deionized water. The mixture was taken together in five pyrex glass dishes in the five different molar ratio *viz*. 1:1, 0.8:0.2, 0.6:0.4, 0.4:0.6 and 0.2:0.8. In order to attain the clear solutions, a stoichiometric ratio of ascorbic acid (Fluka, AR grade) was added to the prepared solutions while stirring until it gets mixed well. Then, the dishes with the above solution are transferred to the modified common microwave oven (Samsung, India Ltd., MG23F301T, 2.45 GHz, 800 W). Initially, the solution gets boiling and started to dehydrate. Then the reaction underwent decomposition and breaks down by releasing gases like N_2, CO_2, H_2O and traces of NO_2 which resulted in light yellow residues. The entire process has taken about 10 min time from the evaporation of liquid to the production of a large quantity of ceria-zirconia powder. The reproducibility of the experiment was confirmed by repeating the procedure in identical conditions and similar properties were attained.

Characterization: The IR spectra were acquired using an FT-IR spectrophotometer (IR Prestige-21, Shimadzu) and the UV-visible spectra were obtained using a double beam UV-Vis. spectrophotometer (UV-1800, Shimadzu) equipped with UV-Probe software. The Shimadzu lab X-6000 diffractometer with Cu$K\alpha$ radiation (λ = 1.54 Å) was used to record X-ray diffraction patterns. The SEM images were captured using a JEOL model JSM 6390 SEM with a 20 kV accelerating voltage. The Raman spectra were collected using a Raman spectrometer (Horiba-Jobin, LabRAM HR) with a spectral range of 50-3000 cm^{-1} and the sources He-Ne (632 nm) and argon (514 nm).

Antimicrobial studies: The antibacterial activity of the prepared nanoparticles was evaluated against two Gram-negative bacterial strains, *Escherichia coli* and *Klebsiella pneumonia* and two Gram-positive bacterial strains, *Staphylococcus aureus* and *Enterococcus faecalis*. Furthermore, the antifungal activity of *Aspergillus niger*, *Penicillium* and *Candida albicans* was also investigated.

***in vitro* Antibacterial assay by agar diffusion method:** Four species *viz*. *Escherichia coli* (MTCC443), *Klebsiella pneumonia* (MTCC530), *Staphylococcus aureus* (MTCC96) and *Enterococcus faecalis* (MTCC439) were selected for this study. Bacteria from the glycerol-frozen stock were disseminated on to blood agar plates and allowed to grow over night at 37 ºC. A 1×10^6 CFU/mL of cells were suspended in Mueller-Hinton broth at 37 ºC and 200 rpm in an incubator. After diluting the bacteria in broth at 10^5 CFU/100 mL, they were added to 100 mL of diluted sample stock solution. The sample stock solution was made by dissolving 10 g of substance in 1 mL of DMF and then diluting it to various concentrations. Before calculating the MIC as the lowest concentration with clean wells, the plate was incubated at 37 ºC for 48 h. The MBC of the samples was measured by plating the wells with a growth inhibitor and noted the lowest concentration at which no growth occurred [23,24].

***in vitro* Antifungal assay by plate dilution method:** The antifungal activity of ceria-zirconia nanoparticles were tested *in vitro* using the plate dilution method [25,26] with minor dilution changes and petri plates. Approximately 1 L of the standardized fungal spore suspension (1×10^7 spores/mL) was carefully liquidated with ceria-zirconia nanoparticles at different concentrations and allowed to diffuse in the media. As positive and negative test controls, the antifungal fluconazole (1.5 µg/mL) and 2 mL of 2% DMSO were utilized. For 7 days, the plates were incubated at 20 ± 2 ºC and fungal growth (mm) in each plate was measured and averaged. To achieve statistical significance, the assay was performed in triplicate and the fungal growth inhibition % was computed with reference to the negative control using a following formula [27]:

$$\text{Fungal growth inhibition } (\%) = \frac{A - B}{A}$$

where A = growth in the negative control (mm); and B = growth in treatment (mm).

The minimum inhibitory of the ceria-zirconia nanoparticles inhibiting the visible fungal growth after incubation time was recorded.

RESULTS AND DISCUSSION

Ultraviolet-visible studies: The UV-visible analysis used for the quantitative determination of the five prepared ceria-zirconia *viz*. CZAA-0, CZAA-1, CZAA-2, CZAA-3 and CZAA-4 nanoparticles and the spectra is shown in Fig. 1. The crystalline cerium oxide possesses a band gap of 3.0 eV and an absorption threshold in the UV-visible region of approximately 400 nm. ZrO_2 had a UV-visible absorption wavelength of 240 nm, which was significantly longer than most other substances. Due to the introduction of zirconium oxide as dopant, the band gap of the ceria crystal lattice observed a shifts blue and a single peak corresponding to cerium oxide is shifted to 252 nm. In particular for cerium and zirconium, it has been demonstrated that the wavelength of UV-visible absorption is quite sensitive to particle size [20]. Between 250 and 340 nm, broad bands were observed in the spectra of ceria-zirconia mixed oxides, which is in fully agreement with the literature [21].

As a result of the charge-transfer transition from O_2^- (2*p*) to Ce^{4+} (4*f*) orbitals in cerium oxide, the absorption spectra of all synthesized ceria-zirconia mixed oxides exhibit a strong absorption band below 400 nm. The increasing zirconium

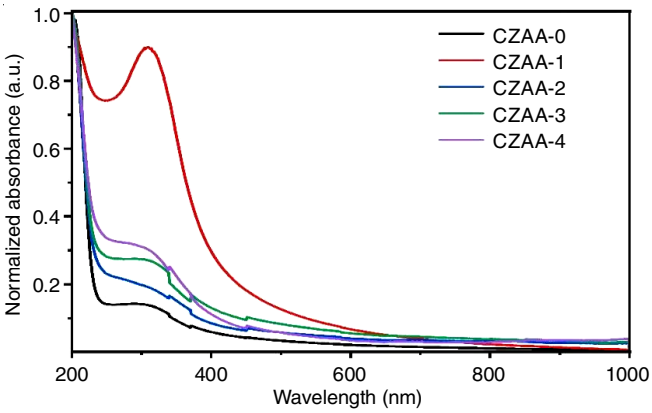

Fig. 1. UV-visible spectra of ceria-zirconia nanoparticles

dopant concentration generates a red shift in the absorption spectra due to the interface polar on effect caused by electron-phonon coupling [22]. Fig. 1 depicts the UV-visible spectra of nanoparticles where an increase in zirconium dopant concentration results in a red shift. The band gap in CZAA-0, CZAA-1, CZAA-2, CZAA-3 and CZAA-4 decreased to 4.92, 4.27, 4.11, 4.02 and 3.95, respectively, as a result of the observed charge transfer transition. Thus, an increase in Zr content tends to minimize the band gap because Zr^{4+} ions substituted in the cerium lattice generate more oxygen vacancies and encourage the formation of Ce^{3+} from Ce^{4+} [28].

FT-IR studies: Fig. 2 depicts the FT–IR spectra of CZAA-0, CZAA-1, CZAA-2, CZAA-3 and CZAA-4 nanoparticles. A broad band around 3395 cm^{-1} was observed, which corresponds to the stretching vibration of hydroxyl groups [29]. The vibrations corresponding to the bands at 1628 and 1381 cm^{-1} are H_2O bending and Ce-OH stretching, respectively. In the instance of cerium-oxygen bonds and zirconium-oxygen bonds, the bands at around 740 and 540 cm^{-1} were ascribed to the Ce-O and Zr-O bonds, respectively. Clark *et al.* [30] reported that the asymmetric Zr-O-Zr stretching will be active in 650-600 cm^{-1} whereas the symmetric stretching of same will appear in the 550-400 cm^{-1} region. In general, the transverse and longitudinal modes of vibrations occur between 650 and 400 cm^{-1} are linked with oxide ion transitions.

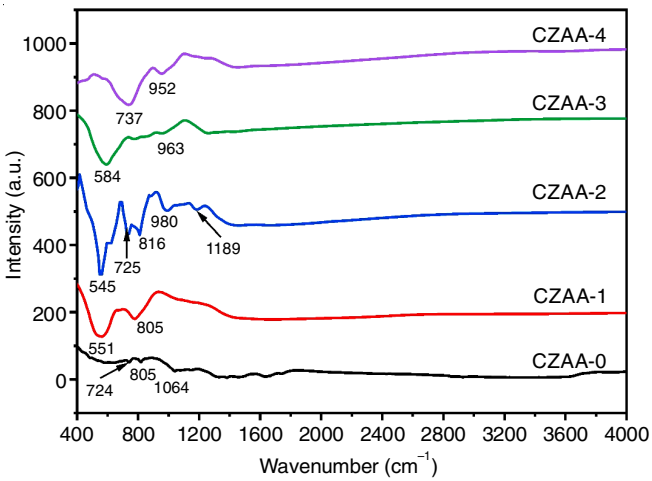

Fig. 2. FT-IR spectra of ceria-zirconia nanoparticles

XRD studies: A well-defined crystalline nature of the prepared nanoparticles is shown by the pattern of XRD peaks with high intensity (Fig. 3). The typical size of a crystallite is 67.29 nm. The diffraction peaks were identified using the crystallographic planes (111), (200), (220), (311), (400) and (331) of CeO_2 with a cubic phase structure (JCPDS card No. 89-8436) [23]. The diffraction peaks at 2θ = 29.19º, 33.50º, 48.50º and 57.49º correspond to the prepared ceria-zirconia nanoparticles, demonstrated that the nanoparticle is evenly dispersed in the structure to form a homogeneous solid solution. Compared to pure ceria, the high 2θ values from XRD indicate the presence of a zirconia-rich phase of minute proportions. Zr^{4+}, which has a smaller ionic radius than Ce^{4+} (0.97), causes a peak shift towards the higher 2θ values [24]. The inclusion of zirconium ion into the ceria unit cell reduces cell properties and induces lattice contraction. All diffraction patterns display large peaks, indicating that the ceria-zirconia nanoparticles synthesized are nanocrystalline in nature.

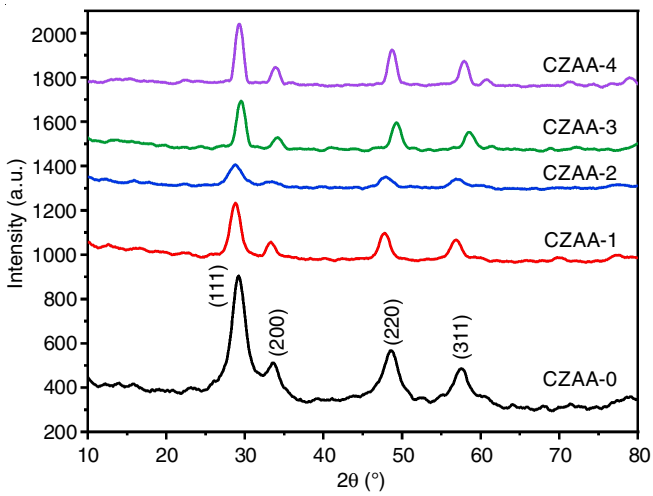

Fig. 3. XRD patternof (a) CZAA-0 (b) CZAA-1 (c) CZAA-2 (d) CZAA-3 (e) CZAA-4

Literature suggests that the microwave-prepared ceria-zirconia nanoparticles have a smaller specific surface area as a result of the sample being exposed to higher temperatures for a shorter period of time during synthesis. Because weakly bound active oxygen species are located in the bulk of cerium oxide rather than its surface, specific surface area is not the only factor affecting the catalytic efficiency of ceria-based solid solutions [25]. Ceria crystallizes as cubic fluorite, exhibiting the most thermodynamically stable surface (111). This surface is the oxygen terminal of the stacked stoichiometric O-Ce-O trilayers in the (111) direction and corresponds to a significant portion of the active surface of catalytic nanocrystalline. For cubic indexation and measurement of unit cell properties, the most intense line (111) of the XRD pattern was utilized. XRD data [26] indicate that the cell parameter decreases, indicating that more Zr^{4+} cations have incorporated into the ceria core FCC lattice (space group *Fm3m*) in the sample.

SEM studies: According to the SEM images (Fig. 4a-b), the particle aggregation occurs and thus showing densely packed agglomerated crystallites. Due to the break down of

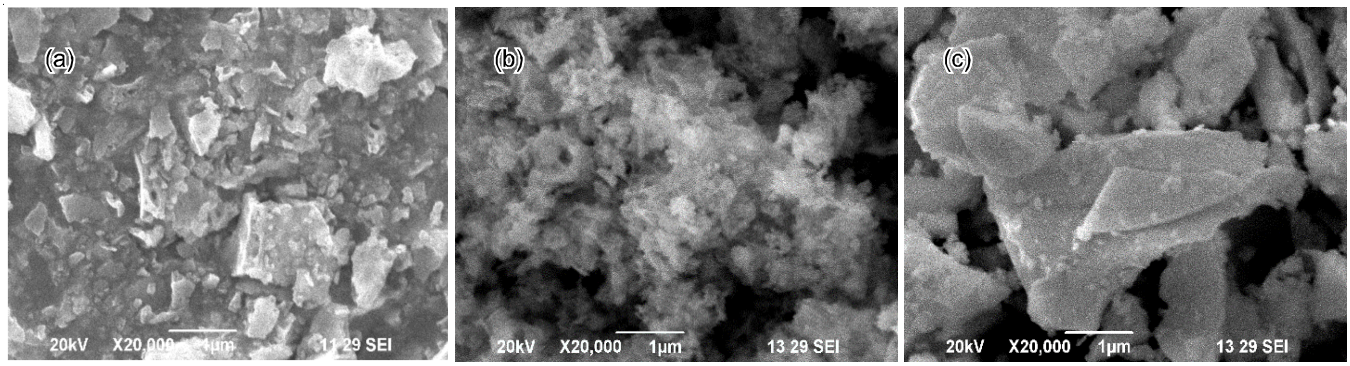

Fig. 4. SEM images of ceria-zirconia nanoparticles

structure after microwave heating [27], the particles have an irregularly formed flake structure and a greater size (Fig. 4c).

Antibacterial activities: At three different concentrations of 25, 50 and 100 mg of ceria-zirconia nanoparticles, antibacterial activity against two Gram-positive and Gram-negative bacterial pathogens were examined. The greatest effect inhibition zones of *E. coli* were 8 mm, *K. pneumonia* was 6 mm, *S. aureus* was 19 mm and *E. faecalis* was 9 mm for 100 mg ceria-zirconia nanoparticles. It was found that 100 mg concentration of the prepared nanoparticles is superior than 25 and 50 mg concentrations in terms of antibacterial activity (Fig. 5).

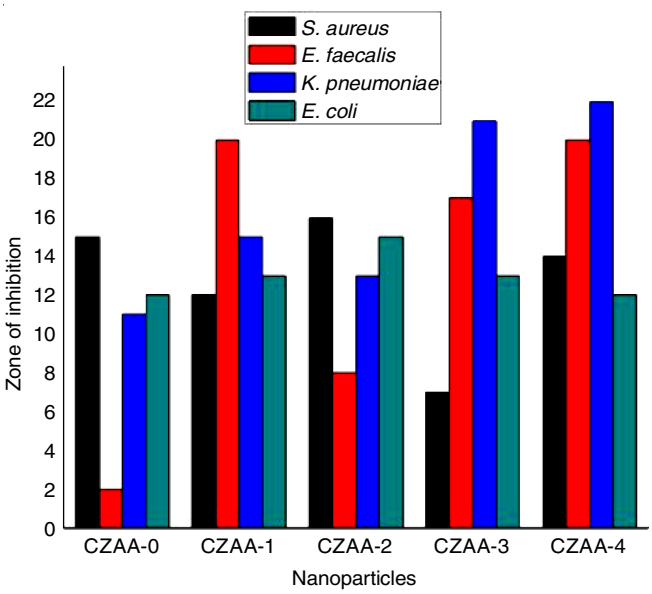

Fig. 5. Antibacterial activities of ceria-zirconia nanoparticles

Due to a reduced particle size of 43.40 nm, sample CZAA-2 nanoparticles showed a remarkable activity against *S. aureus* and *E. coli*. Despite the larger particle size (114.5 nm) of sample CZAA-4, the zone of inhibition was observed and this activity may be due to the sensitivity of nanoparticles linked with the various cell wall architectures of bacteria and fungus.

Antifungal activities: Fig. 6 represents the antifungal activity of ceria-zirconia nanoparticles produced against *A. niger*, *C. albicans* and *Penicillium*. The ceria-zirconia nanoparticles possesses significant antifungal properties against a variety of fungal pathogens. Different concentrations of ceria-

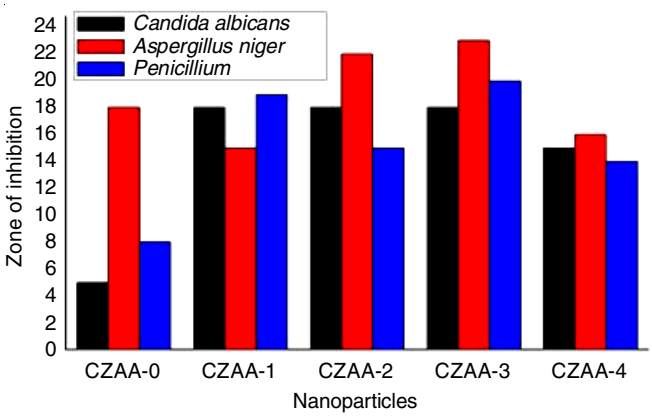

Fig. 6. Antifungal activities of ceria-zirconia nanoparticles

zirconia nanoparticles (1.00, 0.50 and 0.25 mg) were employed for the antifungal activity. At 30 mm and 21 mm, the zone of inhibition for *A. niger* and *Penicillium* was higher than for *Candida albicans*.

The fungicidal activity of ceria-zirconia nanoparticles was greatest against *Aspergillus niger*, with an inhibition zone of 28 mm demonstrating its potency as an antifungal agent. The antimicrobial potential of metal oxide nanoparticles is likely due to electromagnetic interaction and ROS generation [31], including the production of lethal hydroxyl radical ($OH^{\bullet}$) when in close proximity to the lipid membrane. The ceria-zirconia nanoparticles may therefore inhibit the growth of fungal strains by interfering with cell activity and inducing hyphal deformation [32].

Conclusion

In present study, a cost-effective single-step microwave assisted approach for the synthesis of ceria-zirconia nanoparticles in different mole ratio and using ascorbic acid as promotor was carried out. More zirconium is incorporated into the ceria lattice and more defective sites were formed during the microwave synthesized sample as observed by XRD studies. Moreover, SEM studies revealed that after being subjected to microwave irradiation, the structure of the prepared nanoparticles collapsed, revealing irregularly shaped and larger ceria-zirconia nanoparticles. Antibacterial activity of the prepared nanoparticles was best against *S. aureus*, whereas antifungal activity was moderate against *A. niger*, *Penicillium* and *C. albicans*.

CONFLICT OF INTEREST

The authors declare that there is no conflict of interests regarding the publication of this article.

REFERENCES

1. Y. Xia, Y. Xiong, B. Lim and S.E. Skrabalak, *Angew. Chem. Int. Ed.*, **48**, 60 (2009); https://doi.org/10.1002/anie.200802248
2. K. Esumi, K. Miyamoto and T. Yoshimura, *J. Colloid Interface Sci.*, **254**, 402 (2002); https://doi.org/10.1006/jcis.2002.8580
3. L. Xia, H. Wang, J. Wang, K. Gong, Y. Jia, H. Zhang and M. Sun, *J. Chem. Phys.*, **129**, 134703 (2008); https://doi.org/10.1063/1.2987705
4. O.V. Salata, *J. Nanobiotechnol.*, **2**, 3 (2004); https://doi.org/10.1186/1477-3155-2-3
5. I. Pastoriza-Santos and L.M. Liz-Marz'an, *Langmuir*, **18**, 2888 (2002); https://doi.org/10.1021/la015578g
6. C.M. Gonzalez, Y. Liu and J.C. Scaiano, *J. Phys. Chem. C*, **113**, 11861 (2009); https://doi.org/10.1021/jp902061v
7. B. Yin, H. Ma, S. Wang and S. Chen, *J. Phys. Chem. B*, **107**, 8898 (2003); https://doi.org/10.1021/jp0349031
8. S.S. Shankar, A. Ahmad and M. Sastry, *Biotechnol. Prog.*, **19**, 1627 (2003); https://doi.org/10.1021/bp034070w
9. D. Adam, *Nature*, **421**, 571 (2003); https://doi.org/10.1038/421571a
10. D.M.P. Mingos and D.R. Baghurst, *Chem. Soc. Rev.*, **20**, 1 (1991); https://doi.org/10.1039/cs9912000001
11. G. Majetich and R. Hicks, *J. Microw. Power Electromagn. Energy*, **30**, 27 (1995); https://doi.org/10.1080/08327823.1995.11688258
12. S.A. Galema, *Chem. Soc. Rev.*, **26**, 233 (1997); https://doi.org/10.1039/cs9972600233
13. A. De la Hoz, A. Diaz-Ortiz and A. Moreno, *Chem. Soc. Rev.*, **34**, 164 (2005); https://doi.org/10.1039/B411438H
14. S. Dey, S. Sun and N.S. Mehta, *Carbon Capture Sci. Technol.*, **1**, 100013 (2021); https://doi.org/10.1016/j.ccst.2021.100013
15. S. Biswas, A. Pal and T. Pal, *RSC Adv.*, **10**, 35449 (2020); https://doi.org/10.1039/D0RA06168A
16. V. Sajith, M. Sandhya and C.B. Sobhan, An Investigation into the Effect of Inclusion of Cerium Oxide Nanoparticles on the Physicochemical Properties of Diesel Oil, In: Proceedings of the ASME International Mechanical Engineering Congress and Exposition (ASME IMECE '06), ASME Materials Division Publication, pp. 1-6 (2006).
17. A. Tarancon, G. Dezanneau, J. Arbiol, F. Peiro and J.R. Morante, *J. Power Sources*, **118**, 256 (2003); https://doi.org/10.1016/S0378-7753(03)00091-0
18. S.A. Ghom, C. Zamani, S. Nazarpour, T. Andreu and J.R. Morante, *Sens. Actuators B Chem.*, **140**, 216 (2009); https://doi.org/10.1016/j.snb.2009.02.078
19. A.G. Frangoul, K.B. Sundaram and P.F. Wahid, *J. Vac. Sci. Technol. B*, **9**, 181 (1991); https://doi.org/10.1116/1.585285
20. M. Das, S. Patil, N. Bhargava, J.-F. Kang, L.M. Riedel, S. Seal and J.J. Hickman, *Biomaterials*, **28**, 1918 (2007); https://doi.org/10.1016/j.biomaterials.2006.11.036
21. A. Cabanas, J.A. Darr, E. Lester and M. Poliakoff, *J. Mater. Chem.*, **11**, 561 (2001); https://doi.org/10.1039/B008095K
22. J. Liu, Z. Zhao, Y.S. Chen, C.M. Xu, A.J. Duan and G.Y. Jiang, *Catal. Today*, **175**, 117 (2011); https://doi.org/10.1016/j.cattod.2011.05.023
23. R. Bakkiyaraj, M. Balakrishnan, G. Bharath and N. Ponpandian, *J. Alloys Compd.*, **724**, 555 (2017); https://doi.org/10.1016/j.jallcom.2017.07.049
24. G. Ren, D. Hu, E.W.C. Cheng, M.A. Vargas-Reus, P. Reip and R.P. Allaker, *Int. J. Antimicrob. Agents*, **33**, 587 (2009); https://doi.org/10.1016/j.ijantimicag.2008.12.004
25. V. Duraipandiyan and S. Ignacimuthu, *Asian Pac. J. Trop. Biomed.*, **1**, S204 (2011); https://doi.org/10.1016/S2221-1691(11)60157-3
26. Y. Abou-Jawdah, H. Sobh and A. Salameh, *J. Agric. Food Chem.*, **50**, 3208 (2002); https://doi.org/10.1021/jf0115490
27. G.R. Rao and H.R. Sahu, *Proc. Indian Acad. Sci. Chem. Sci.*, **113**, 651 (2001).
28. K.A. Bhabu, J. Theerthagiri, J. Madhavan, T. Balu, G. Muralidharan and T.R. Rajasekaran, *J. Mater. Sci. Mater. Electron.*, **27**, 1566 (2016); https://doi.org/10.1007/s10854-016-5214-x
29. S Letichevsky, C.A. Tellez, R.R. de Avillez, M.I.P. da Silva, M.A. Fraga and L.G. Appel, *Appl. Catal. B*, **58**, 203 (2005); https://doi.org/10.1016/j.apcatb.2004.10.014
30. D.E. Clark, I. Ahmad and R.C. Dalton, *Mater. Sci. Eng. A*, **144**, 91 (1991); https://doi.org/10.1016/0921-5093(91)90213-7
31. T. Xia, M. Kovochich, M. Liong, L. Mädler, B. Gilbert, H. Shi, J.I. Yeh, J.I. Zink and A.E. Nel, *ACS Nano*, **2**, 2121 (2008); https://doi.org/10.1021/nn800511k
32. S. Gowri, R. Rajiv Gandhi and M. Sundrarajan, *Mater. Sci. Technol.*, **30**, 782 (2014); https://doi.org/10.1016/j.jmst.2014.03.002